Biochemistry and Biophysics Reports 26 (2021) 100957

Contents lists available at ScienceDirect

Biochemistry and Biophysics Reports

journal homepage: www.elsevier.com/locate/bbrep

Transferrin-based radiolabeled probe predicts the sensitivity of human renal cancer cell lines to ferroptosis inducer erastin

Yuki Shibata [a,b], Hironobu Yasui [a,b,c,*], Kei Higashikawa [a,b], Yuji Kuge [a,b]

[a] Department of Biomedical Imaging, Graduate School of Biomedical Science and Engineering, Hokkaido University, Sapporo, Hokkaido, 060-8638, Japan
[b] Central Institute of Isotope Science, Hokkaido University, Sapporo, Hokkaido, 060-0815, Japan
[c] Laboratory of Radiation Biology, Department of Applied Veterinary Sciences, Graduate School of Veterinary Medicine, Hokkaido University, Sapporo, Hokkaido, 060-0818, Japan

ARTICLE INFO

Keywords:
Ferroptosis
Transferrin
Transferrin Receptor-1
Gallium-68
Renal cancer
Erastin

ABSTRACT

Ferroptosis induction has been recognized as a novel cancer therapeutic strategy. To effectively apply ferroptosis-targeting cancer therapy to individual patients, a diagnostic indicator for selecting this therapeutic strategy from a number of molecular targeting drugs is needed. However, to date, methods that can predict the efficacy of ferroptosis-targeting treatment have not been established yet. In this study, we focused on the iron metabolic pathway to develop a nuclear imaging technique for diagnosing the susceptibility of cancer cells to ferroptosis. As a nuclear probe, human transferrin (Tf) was labeled with Gallium-68 (^{68}Ga) using 2-(p-isothiocyanatobenzyl)-1,4,7-triazacyclononane-1,4,7-triacetic acid (NOTA) as a chelator (^{68}Ga-NOTA-Tf). Western blot assay and clonogenic survival assay with human renal cancer cell lines A498 and 786-O revealed that the protein expression level of transferrin receptor1 (TfR1) and sensitivity to a ferroptosis inducer, erastin, were correlated. A cellular uptake assay with ^{68}Ga-NOTA-Tf revealed that the cancer cells sensitive to erastin highly internalized the ^{68}Ga-NOTA-Tf. Furthermore, treatment with the TfR1 inhibitor ferristatin II reduced the cellular uptake of ^{68}Ga-NOTA-Tf, indicating that the intracellular uptake of the probe was mediated by TfR1. These results suggest that ^{68}Ga-NOTA-Tf can be useful in predicting the sensitivity of cancer cells to ferroptosis inducers.

1. Introduction

Therapeutic resistance in cancer remains a serious issue in clinical practice. One conceivable cause for therapeutic resistance is that cancer cells with genomic instability can easily acquire resistance to drugs through adaptive responses, thus reducing therapeutic effects [1,2]. To overcome this problem, the development of a novel anticancer strategy that induces cancer cell death through a mechanism different from existing drugs is an urgent challenge. Recently, the discovery of ferroptosis, which is a type of cell death induced by iron-dependent lipid peroxide accumulation, has attracted attention as a novel cancer therapy [3]. Iron is an essential nutrient for mammalian organisms. Its important function is to bind with hemoglobin and carry oxygen. Furthermore, iron acts as the active center of various biological enzymes such as cytochrome p450, which is necessary for drug metabolism, and ribonucleotide reductase, which is involved in DNA biosynthesis. On the other hand, iron homeostasis in cancer cells is often disrupted, leading to an excess accumulation of iron [4]. This is because cancer cells significantly increase the uptake of iron for upregulating the iron-dependent enzyme ribonucleotide reductase and accelerating their proliferation [5]. In other words, cancer cells with excess iron are considered more likely to induce ferroptosis than normal cells. Recent studies have demonstrated that some tumors were suppressed by the treatment of several ferroptosis inducers, indicating that ferroptosis induction may be a useful approach for cancer therapy [6,7].

Due to the diversity of cancers, the sensitivity to ferroptosis inducers is expected to differ depending on the cancer type [8,9]; therefore, therapeutic effects are naturally expected to vary among patients. However, there is still no method for predicting and monitoring the efficacy of ferroptosis-inducing agents. To effectively adapt ferroptosis-targeting therapy to individual patients, development of a technique for predicting the sensitivity of cancer to therapy is required. To date, there are no studies that have established a promising tool for predicting ferroptosis sensitivity. Since lipid peroxides are produced by intracellular iron as a trigger for ferroptosis, a major iron uptake

* Corresponding author. Laboratory of Radiation Biology, Department of Applied Veterinary Sciences, Graduate School of Veterinary Medicine, Hokkaido University, Kita 18, Nishi 9, Kita-ku, Sapporo, Hokkaido, 060-0818, Japan.
E-mail address: yassan@vetmed.hokudai.ac.jp (H. Yasui).

https://doi.org/10.1016/j.bbrep.2021.100957
Received 29 June 2020; Received in revised form 14 February 2021; Accepted 15 February 2021

List of abbreviations

aTf	apo transferrin
DMSO	dimethyl sulfoxide
EDTA	ethylenediaminetetraacetic acid
^{68}Ga	Gallium-68
GPX4	glutathione peroxidase 4
HEPES	2-[4-(2-hydroxyethyl) piperazin-1-yl] ethanesulfonic acid
HPLC	high-performance liquid chromatography
hTf	holo transferrin
ICP-AES	inductively coupled plasma atomic emission spectrometry
MALDI-TOF-MS	matrix-assisted laser desorption-ionization time-of-flight mass spectrometry
NOTA	p-isothiocyanatobenzyl-1,4,7-triazacyclononane-1,4,7-triacetic acid
PBS	phosphate-buffered saline
ROS	reactive oxygen species
SDS-PAGE	sodium dodecyl sulfate polyacrylamide gel electrophoresis
Tf	transferrin
TLC	thin-layer chromatography
TfR	transferrin receptor
xCT	cystine/glutamate antiporter

pathway via transferrin-transferrin receptor (Tf-TfR) complex can be considered a key factor for cancer sensitivity to ferroptosis inducers. Studies indicate that the serum iron transporter transferrin plays a crucial role in ferroptosis induction and the expression level of TfR1 protein in cancer cells, which is closely correlated with sensitivity to ferroptosis-inducers [10,11]. Therefore, we hypothesized that the amount of Tf taken up by cells correlates with cancer sensitivity to erastin, an inducer of ferroptosis [10]. With the aim of developing a prediction method for cancer sensitivity to ferroptosis-inducing drugs, a radiolabeled probe that can measure Tf uptake levels in cancers was evaluated in this study [12].

2. Materials & methods

2.1. Reagents

Erastin was purchased from AdooQ Bioscience (Cat. No. A13822, Irvine, CA). Ferristatin II (also called chlorazol black) was purchased from Tokyo Chemical Industry Co. (Cat. No. C0533, Tokyo, Japan). Human apo-transferrin (aTf, Cat. No. T2036) and human holo-transferrin (hTf, Cat. No. T0665) were purchased from Sigma-Aldrich (St. Louis, MO). The following antibodies were used for western blotting: rabbit anti-TfR1 (Cat. No. ab84036, Abcam, Cambridge, UK), mouse anti-α-tubulin (Cat. No. T9026, Sigma-Aldrich), mouse anti-β-actin (Cat. No. A3854, Sigma-Aldrich), and horseradish peroxidase-conjugated anti-rabbit and anti-mouse secondary antibodies (Cat. Nos. W401B and W402B, Promega, Madison, WI).

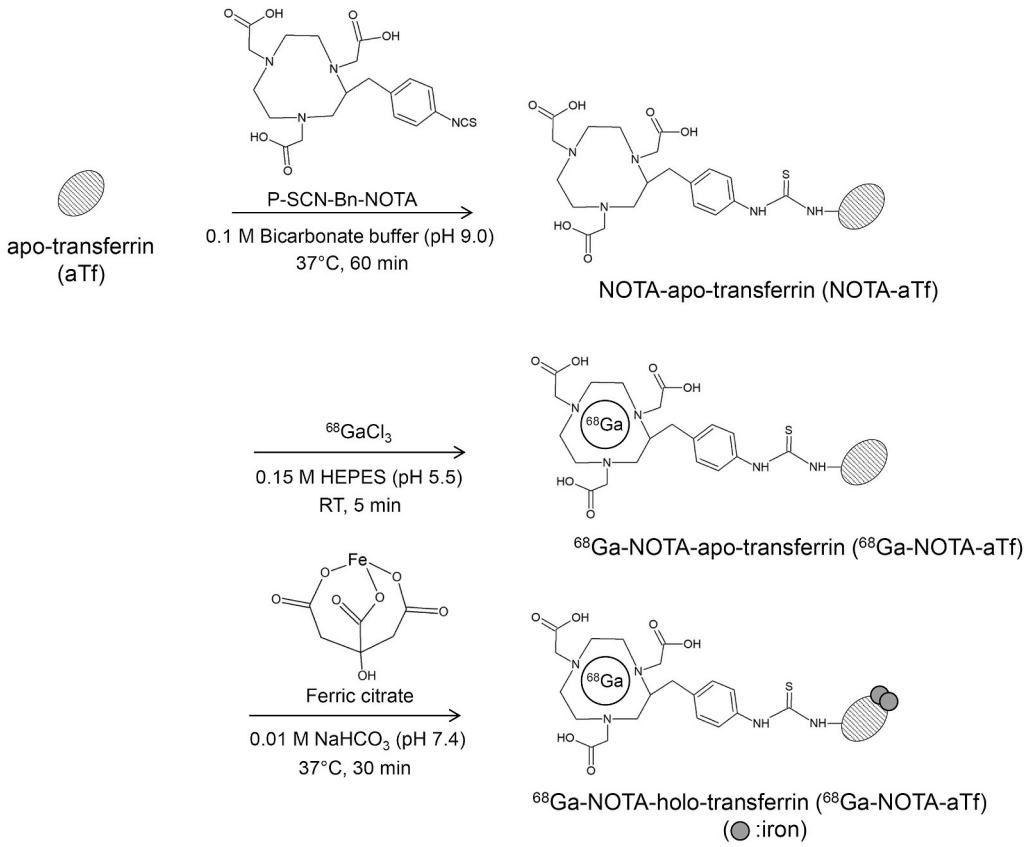

Fig. 1. Synthetic pathway for the ^{68}Ga-NOTA-hTf.
The synthesis of ^{68}Ga-NOTA-hTf was carried out in three reaction steps. Human-apo-transferrin and NOTA were conjugated through an isothiocyanate moiety. ^{68}Ga-NOTA-hTf (iron-bound form) was synthesized by reacting ^{68}Ga-NOTA-aTf with an excess amount of ferric citrate.

2.2. Conjugation of p-isothiocyanatobenzyl-1,4,7-triazacyclononane-1,4,7-triacetic acid (NOTA) to aTf

The conjugation of NOTA to aTf was performed using the method reported by Bhattacharyya et al. [13]. The synthesis scheme for gallium-68 (^{68}Ga)-NOTA-transferrin is illustrated in Fig. 1. As the first step, NOTA-aTf was synthesized by mixing aTf (1.0 mg/mL) in 0.1 M carbonate buffer (pH 9.0) with a 16-fold molar excess of p-isothiocyanatobenzyl-NOTA (Cat. No. B-605, Macrocyclics, Inc., Plano, TX) in DMSO for 1 h at 37 °C. The DMSO concentration was below 5% in this reaction mixture. NOTA-aTf was purified and the solvent was replaced with phosphate-buffered saline (PBS) (−) with a PD-10 column (GE Healthcare Life Sciences, Buckinghamshire, UK) and an Amicon Ultra 50K device (Merck Millipore, Burlington, MA).

2.3. Radiolabeling and hTf formation

Radiolabeling of ^{68}Ga was conducted according to the method described in previous papers [14,15]. $^{68}GaCl_3$ was eluted from a ^{68}Ge/^{68}Ga-generator (Galli Eo®, IRE ELiT, Fleurus, Bergium). The $^{68}GaCl_3$ solution was evaporated and resolved in 10 μL of 0.1 M HCl. The solvent (phosphate buffer) of NOTA-aTf was replaced with 0.1 M 2-[4-(2-hydroxyethyl) piperazin-1-yl] ethanesulfonic acid (HEPES) (pH 5.5) using an Amicon Ultra 50K device. The $^{68}GaCl_3$ solution (c.a. 10 μL) was added to the NOTA-aTf solution and adjusted to 1.0 mg/mL with 0.1 M HEPES buffer. The mixture was incubated at 25 °C for 5 min to obtain NOTA-aTf labeled with ^{68}Ga (^{68}Ga-NOTA-aTf). After incubation, the solvent was replaced with 0.01 M $NaHCO_3$ (pH 7.4) using the Amicon-Ultra 50K device. To saturate the ^{68}Ga labeled NOTA-aTf with iron completely, ^{68}Ga-NOTA-aTf was reacted with an excess amount of $FeCl_3$ (same volume of 2 mM $FeCl_3$ and 40 mM citric acid solution [pH 7.4]) at 37 °C for 30 min [14]. The synthesized ^{68}Ga-NOTA-aTf and ^{68}Ga-NOTA-hTf were purified with a PD-10 column, and the solvent was replaced with PBS (−) with an Amicon Ultra 50K device. The resultant solution was used for the *in vitro* uptake study.

The radiochemical purities of ^{68}Ga-NOTA-aTf and ^{68}Ga-NOTA-hTf were confirmed by radio-thin layer chromatography (TLC) and high-performance liquid chromatography (HPLC) analyses. TLC analysis was performed using reversed-phase TLC plates (RP-18 F254 S, Merck Millipore) and 0.02 M citric acid- 0.05 M ethylenediaminetetraacetic acid (EDTA) (pH 5.0) as the mobile phase. TLC chromatograms were obtained by autoradiography (FLA-7000IR; GE Healthcare Life Science, Buckinghamshire, UK). Size exclusion HPLC was performed with a TSKgel SuperSW2000 column (Tosoh Bioscience LLC, King of Prussia, PV) connected to a TSKgel SuperSW guard column (Tosoh Bioscience LLC, King of Prussia, PV); phosphate buffer (0.3 M NaCl, 0.01 M phosphate buffer [pH 7.0]) was used as the mobile phase (flow rate, 0.4 mL/min; wavelength, 280 nm). The chromatograms were obtained using an HPLC system equipped with a multi-wavelength UV detector (SPD-20A UV/VIS detector, Shimadzu, Tokyo, Japan) and a radioactivity detector (Raytest Gabi Star, Straubenhardt, Germany).

2.4. Number of chelators conjugated with aTf

Matrix-assisted laser desorption-ionization time-of-flight mass spectrometry (MALDI-TOF-MS) was performed using an ultrafleXtreme (Bruker Daltonics, Bremen, Germany) to examine the number of chelators conjugated with aTf. Non-conjugated- and chelator-conjugated aTf were desalted using PD Spin Trap G-25 (GE Healthcare Life Science). 3,5-Dimethoxy-4-hydroxycinnamic acid (Tokyo Chemical Industry Co.) at 10 mg/mL in 1:1 acetonitrile/H_2O with 0.1% trifluoroacetic acid was used as the MALDI matrix. For each sample, measurements were repeated four times. The measured mass difference between aTf and NOTA-aTf was divided by the mass value of single NOTA, and the resulting values represented the average number of NOTA that were conjugated to aTf.

2.5. Iron concentration

The concentration of transferrin-bound iron was determined by multiple inductively coupled plasma atomic emission spectrometry (ICP-AES) (ICPE-9000, Shimadzu). Before the ICP-AES measurement, each sample (0.5 mg) was pre-digested in 10 mL of 4% ultra-high purity nitric acid (KANTO CHEMICAL Co., Inc., Tokyo, Japan) and heated at 200 °C for 20 min using a microwave digestion system (ETHOS-ONE, Milestone, Sorisole, Italy). The standard curve was prepared with an iron standard solution (AccuStandard Inc., New Haven, CT).

2.6. Cell culture

Human renal cancer cell lines (A498 and 786-O cells) were purchased from American Type Culture Collection (Manassas, VA). These cells were grown in RPMI-1640 medium (Sigma-Aldrich) supplemented with 10% fetal bovine serum (CELLect®, MP Biomedicals, Santa Ana, CA) and 100 units/mL of penicillin-streptomycin (MP Biomedicals), and maintained at 37 °C and 5% CO_2.

2.7. Clonogenic survival assay

The sensitivity of cancers to the ferroptosis inducer erastin was evaluated *in vitro* using a clonogenic survival assay. An appropriate number of cancer cells were seeded into 60 mm dishes and incubated in 5% CO_2 at 37 °C for 6 h. The cells were adhered to the dishes and treated with erastin at the indicated concentrations. After 24 h of erastin treatment, the medium was replaced with fresh erastin-free medium. To form cell colonies, the cells were incubated for 9 days in a humidified 5% CO_2 atmosphere at 37 °C. The colonies were fixed with methanol and stained with Giemsa solution. Surviving colonies containing more than 50 cells were counted under a microscope (CKX41, Olympus, Tokyo, Japan). Each surviving fraction was corrected using the plating efficiency of the non-treated control.

2.8. Sodium dodecyl sulfate polyacrylamide gel electrophoresis (SDS-PAGE) and western blotting

TfR1 protein expression levels in A498 and 786-O cells were analyzed by western blotting. For TfR1 inhibition, cells were cultured for 4 h in serum-free medium containing 0–100 μM ferristatin II, after which cells were collected. The collected samples were dissolved in RIPA buffer (Thermo Fisher Scientific, Carlsbad, CA) containing a protease inhibitor cocktail (Roche Diagnostics, Basel, Switzerland) and underwent a repeated freeze–thaw cycle twice. After centrifuging lysed cells at 15,000×*g* for 20 min at 4 °C, the supernatants were collected as protein samples. The protein samples were mixed with Laemmli's sample buffer (Bio-Rad, Hercules, CA), and the mixture was boiled for 5 min. Samples were separated using SDS-PAGE and transferred onto a polyvinylidene difluoride membrane (Bio-Rad). Protein transfer was performed using a Mini Trans-Blot® Cell (Bio-Rad) at 60 V in transfer buffer (25 mM Tris, 192 mM glycine, and 20% methanol) for 60 min at 4 °C. The membrane was incubated with specific antibodies diluted with TBST (10 mM Tris-HCl [pH 7.4], 0.1 M NaCl, and 0.1% Tween-20) containing 5% skim milk (Wako Pure Chemical Industries, Osaka, Japan) overnight at 4 °C and then incubated for an hour at room temperature. The membrane was probed with HRP-conjugated secondary antibodies, and the antibodies were detected with an Immobilon® western HRP substrate (Merck Millipore). The membrane was scanned using LAS-4000 (Fujifilm, Tokyo, Japan) and densitometry analysis was performed using Multi Gauge V3.0 software (Fujifilm).

2.9. Cell uptake assay

A498 and 786-O cells were plated in 30 mm dishes (2.0×10^5 cells/dish) and incubated overnight at 37 °C in 5% CO_2. For TfR1 inhibition,

the cells were treated with serum-free RPMI-1640 medium containing 50 μM ferristatin II and were incubated for 4 h at 37 °C in 5% CO_2. An aliquot (0.1 mL) of ^{68}Ga-NOTA-aTf or ^{68}Ga-NOTA-hTf (20 μg/mL [2.2–3.1 MBq/mL]) was added to the cells and incubated for an hour. After incubation, the media was removed, and cells were washed twice with PBS (1.0 mL). The cells were then incubated with 1.0 mL of acidic solution (0.1 M glycine, 20 mM acetic acid, pH 4.0) for 1 min to strip surface-bound transferrin. Finally, cells were lysed in 1.0 mL of 0.1 M NaOH (aq.) to collect internalized activity. Radioactivity in the media, wash solution, cell surface, and intracellular fractions were measured using a γ-counter (Wizard 2 2480, Perkin-Elmer, Waltham, MA). After dividing the radioactivity of the intracellular fraction with the sum of all fractions, the data were normalized using the cellular protein amount of each sample quantified with a BSA protein assay and represented as % internalized activity/mg protein. According to the previous study [16] in which the uptake values of ^{125}I-labeled Tf were about 1–3% internalized activity/1 × 10^6 cells, normalization was performed with one mg protein (equivalent to 0.87 × 10^6 cells for 786-O cells and 1.40 × 10^6 cells for A498 cells).

2.10. Statistical analysis

All results are expressed as the mean ± standard deviation (SD) from at least three independent experiments. Statistical analysis was performed using GraphPad Prism 7. Differences in TfR1 protein expression levels between the two cell lines were evaluated using Student's t-test (Fig. 2). The statistical significance of erastin cytotoxicity on the two cell lines was examined using two-way ANOVA (Fig. 2). Multiple comparisons of the results of cellular uptake analysis and western blot analysis with ferristatin II treatment were performed with a Tukey-Kramer test (Figs. 3 and 4). A p-value < 0.05 was considered significant.

3. Results

3.1. Synthesis of ^{68}Ga-NOTA-aTf and ^{68}Ga-NOTA-hTf

The numbers of NOTA conjugated to aTf were measured by MALDI-TOF-MS. The average number of NOTA molecules was 2.66 ± 0.22 per aTf molecule (n = 3). The amount of iron bound to transferrin was measured by ICP-AES. The amount of iron in the ^{68}Ga-NOTA-hTf obtained in the present study was 1133.3 μg/g; the amount of iron in the aTf (starting material) and hTf (purchased standard) was 90.5 and 1048.0 μg/g, respectively. The radiochemical yields of ^{68}Ga-NOTA-aTf and ^{68}Ga-NOTA-hTf were approximately 70% (Table 1). The radiochemical purities of ^{68}Ga-NOTA-aTf and ^{68}Ga-NOTA-hTf, analyzed by TLC and HPLC, were more than 96% and 92%, respectively.

3.2. TfR1 protein expression levels and sensitivity of human renal cancer cell lines to erastin

Fig. 2A shows the expression levels of TfR1 protein in human renal cancer cell lines (A498 and 786-O) analyzed by western blotting. TfR1 expression levels in 786-O cells were significantly higher than those in A498 cells. The sensitivity of 786-O cells to erastin was also found to be significantly higher than that of A498 cells, as revealed by the clonogenic survival assay. The surviving fractions of A498 and 786-O cells treated with 10 μM erastin for 24 h were 19.0% and 2.9%, respectively. (Fig. 2B).

3.3. Cellular uptake assay of ^{68}Ga-NOTA-aTf and ^{68}Ga-NOTA-hTf in renal cancer cell lines

The cellular uptake levels of ^{68}Ga-NOTA-aTf and ^{68}Ga-NOTA-hTf were evaluated. As shown in Figure 3, ^{68}Ga-NOTA-hTf was highly internalized compared to ^{68}Ga-NOTA-aTf in both cell lines (0.60 ± 0.11% vs. 0.32 ± 0.08% in A498, 1.03 ± 0.10% vs. 0.31 ± 0.07% in 786-O). The level of internalized ^{68}Ga-NOTA-hTf was significantly higher in 786-O cells than in A498 cells ($p = 0.0021$).

3.4. Relationship of ferristatin II treatment to TfR1 protein expression level and ^{68}Ga-NOTA-hTf uptake level of renal cancer cell lines

TfR1 protein expression levels in A498 and 786-O cells treated with various concentrations of ferristatin II were analyzed. Western blot analysis showed that 4-h treatment with ferristatin II decreased TfR1 protein in both cell lines (Fig. 4A). Furthermore, the cellular uptake of ^{68}Ga-NOTA-hTf was significantly reduced by pre-treatment with 50 μM ferristatin II in both cell lines (Fig. 4B).

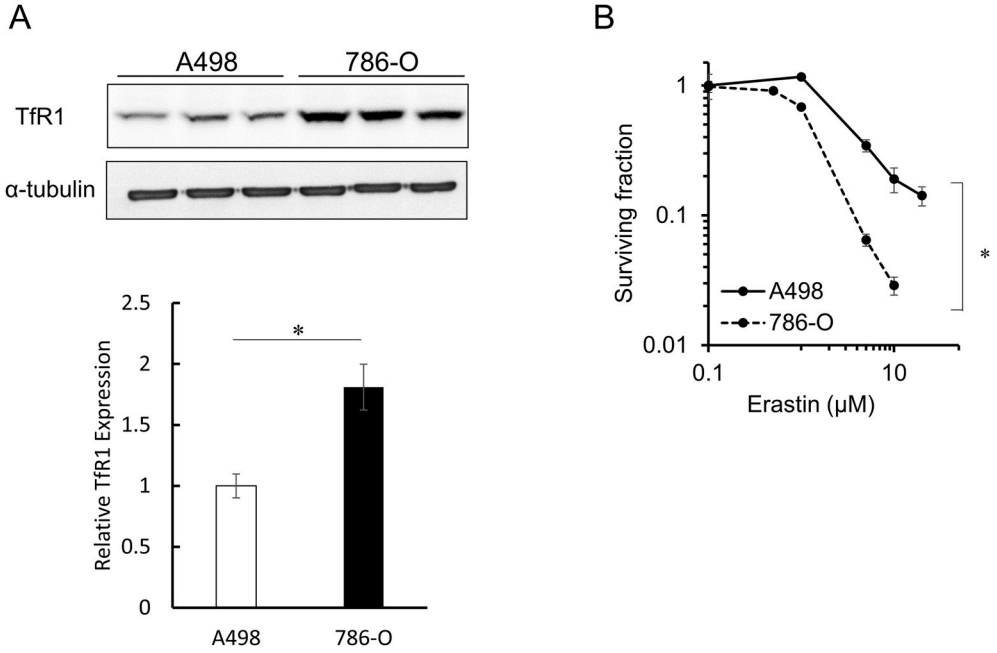

Fig. 2. Comparison of TfR1 protein expression levels and cytotoxicity of erastin in two human renal cancer cell lines. Western blotting for TfR1 and α-tubulin was performed on A498 and 786-O cells. The obtained images were analyzed to calculate the relative TfR1 expression levels in these cell lines. The data is expressed as mean ± SD (n = 3, *$p < 0.01$, Student's t-test) (A). A clonogenic assay was performed on A498 and 786-O cells exposed to erastin. Cancer cells were treated with erastin (0–20 μM) for 24 h. Data is expressed as mean ± SD (n = 3, *$p < 0.05$, two-way ANOVA) (B).

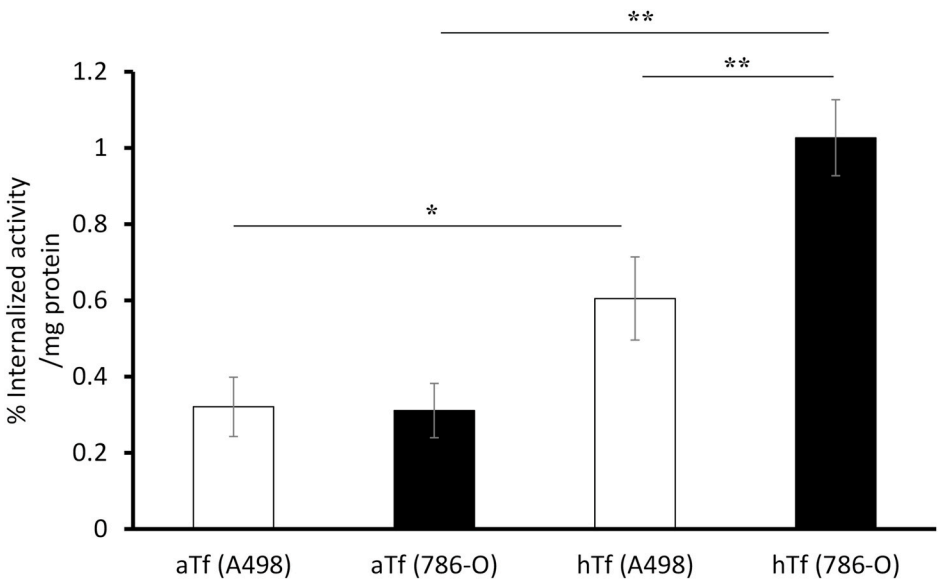

Fig. 3. Cellular uptake of ^{68}Ga-NOTA-aTf and ^{68}Ga-NOTA-hTf in human renal cancer cell lines.
Cell uptake assays of ^{68}Ga-NOTA-aTf and ^{68}Ga-NOTA-hTf were performed with A498 and 786-O cells. Cancer cells were incubated with ^{68}Ga-NOTA-aTf or ^{68}Ga-NOTA-hTf at 37 °C for 60 min. The internalized activity was calculated as described in Materials and Methods and represented as % internalized activity/mg protein. All data is expressed as mean ± SD (n = 3, *$p < 0.05$, **$p < 0.01$, Tukey–Kramer test).

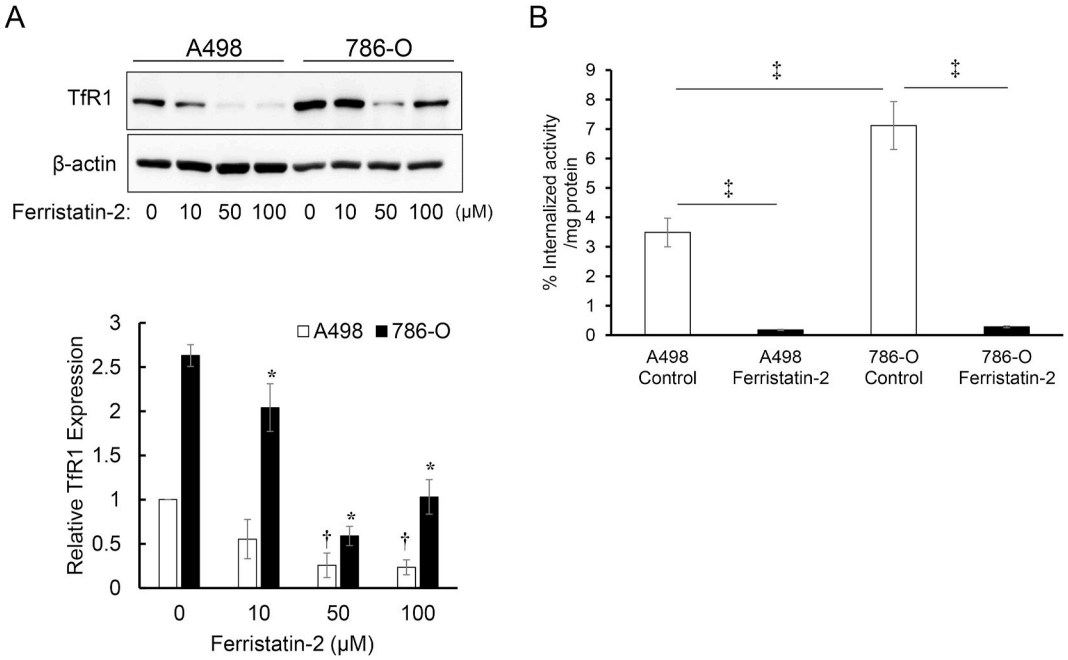

Fig. 4. Effects of ferristatin II on TfR1 protein expression levels and cellular uptake of ^{68}Ga-NOTA-hTf in human renal cancer cell lines.
Inhibitory effects of ferristatin II were evaluated by western blot analysis of TfR1 and β-actin expression in A498 and 786-O cells. The obtained images were analyzed to calculate the relative TfR1 expression levels in these cell lines. The data is expressed as mean ± S.D. Symbol * denotes $p < 0.01$ *vs.* 786-O cells treated with 0 μM ferristatin II. Symbol † denotes $p < 0.01$ *vs.* A498 cells treated with 0 μM ferristatin II (n = 3, Tukey–Kramer test) (A). Cellular uptake of ^{68}Ga-NOTA-hTf after the inhibition of TfR1 expression by ferristatin II treatment was evaluated in A498 and 786-O cells. The internalized activity was calculated by dividing the activity of the intracellular fraction by the sum of all fractions. The data is expressed as mean ± SD (n = 3, ‡$p < 0.01$, Tukey–Kramer test) (B).

Table 1
Radiochemical yields and purities of ^{68}Ga-NOTA-aTf and ^{68}Ga-NOTA-hTf.

^{68}Ga-NOTA-Tf	Apo form	Holo form
Radiochemical yield	72.8%	63.5%
Radiochemical purity (TLC)	>98%	>98%
Radiochemical purity (HPLC)	>96%	>92%
Protein concentration (μg/mL)	20	20
Radioactivity concentration (MBq/mL)	3.1	2.2

The radiochemical purities of ^{68}Ga-NOTA-aTf and ^{68}Ga-NOTA-hTf were confirmed by TLC and HPLC analysis.

4. Discussion

Recently, ferroptosis has attracted attention as a therapeutic target for cancer. Indeed, several ferroptosis inducers attenuate chemotherapy and radiotherapy resistance while enhancing their therapeutic effects [17–19]. Therefore, ferroptosis-targeting cancer therapy is an effective therapeutic strategy that can be used for refractory cancers. However, the sensitivity to the ferroptosis inducer erastin varies among cancer cell types [8], and suppression of TfR1 by siRNA treatment decreases cancer sensitivity to erastin [10]. Moreover, the iron transporter transferrin in serum was found to be essential for ferroptosis induction through amino

acid starvation [20]. Thus, the relationship between ferroptosis and iron metabolic pathways is strongly suggested. In this study, we aimed to obtain preclinical data to establish a method for predicting the efficacy of ferroptosis-targeting anticancer therapy. We developed a radioactive probe targeting TfR1, with ^{68}Ga-labeled human transferrin conjugated with NOTA as a metal chelator. There are two forms of transferrin, namely aTf and hTf. It is known that iron-bound hTf has a higher binding affinity to the receptor than aTf [21]. Therefore, aTf was first conjugated with the metal chelator NOTA and then radiolabeled with ^{68}Ga to synthesize ^{68}Ga-NOTA-aTf. After radiolabeling, ^{68}Ga-NOTA-aTf was reacted with an excess amount of ferric citrate to form ^{68}Ga-NOTA-hTf (Fig. 1).

To clarify the TfR-dependent sensitivity to a ferroptosis inducer, two human renal cancer cell lines that showed significant differences in TfR1 protein expression levels were used in this study (Fig. 2A). The sensitivity of TfR1-highly expressed 786-O cells to erastin was significantly higher than that of TfR1-low expressed A498 cells (Fig. 2B). This result indicates that TfR1 expression levels in human renal cancer cell lines are closely correlated with the sensitivity of cancers to the ferroptosis-inducer erastin. Notably, the internalized amount of ^{68}Ga-NOTA-hTf was significantly higher in 786-O cells than that in A498 cells (Fig. 3). ^{68}Ga-NOTA-aTf showed limited internalization in both cell lines, indicating that iron saturation is necessary for intracellular uptake of radiolabeled NOTA-Tf by cancer cells. By the treatment of ferristatin II as an inhibitor of TfR1 [22], the TfR1 protein expression levels in A498 and 786-O cells were significantly decreased (Fig. 4A) and the cellular uptake of ^{68}Ga-NOTA-hTf was strongly blocked (Fig. 4B). These results confirm the specificity of ^{68}Ga-NOTA-hTf to TfR1. Taken together, our study provides the first evidence suggesting that ^{68}Ga-NOTA-hTf could predict cancer sensitivity to the ferroptosis-inducer erastin.

In this study, ^{68}Ga nuclide was used for radiolabeling transferrin because ^{68}Ga can be easily obtained from a ^{68}Ge/^{68}Ga-generator. Although this positron emission nuclide has recently attracted attention as a useful radionuclide for PET imaging, its short half-life may hamper the diagnostic imaging of labeled compounds with large molecular weights, including transferrin, due to the slow pharmacokinetics of the labeled compound. However, NOTA-hTf can be easily labeled with other radionuclides with longer half-lives, such as ^{67}Ga and ^{64}Cu. This high versatility enables us to evaluate TfR1 function as a prognostic indicator for ferroptosis-targeting therapy non-invasively. Further *in vivo* experiments to investigate the correlation of the accumulation of radiolabeled NOTA-hTf in tumors with the anticancer effect of the ferroptosis inducer are necessary for establishing a diagnostic method of ferroptosis induction in cancer with nuclear medicine imaging. In preliminary experiments, we performed a distribution assay of ^{68}Ga-NOTA-hTf in a 786-O/A498 xenograft model. As a result, the accumulation of ^{68}Ga-NOTA-hTf in tumors was not significantly different between these cell lines (Supplemental Fig 1). This may be because the expression level of TfR1 varies even in the same cell line due to the tumor size and intratumor heterogeneity. Further detailed investigation of TfR1 expression and ^{68}Ga-NOTA-hTf-accumulated regions is warranted.

In the present study, investigations were performed only in human renal cancer cell lines. Thus, it is unclear whether similar results can be obtained with cancer cells derived from organs other than the kidney. Several reports have shown that the sensitivities of HRAS-mutant cancers and leukemia cell lines to ferroptosis induction are correlated with TfR1 and cellular labile iron pools [10,23,24]. Therefore, it can be hypothesized that results similar to those in this study are likely to be obtained for further studies on cell types derived from other organs.

In conclusion, radiolabeled NOTA-hTf may have the potential to predict the therapeutic effect of ferroptosis-targeting cancer therapy *in vitro*. By diagnosing the therapeutic effect of ferroptosis-targeting cancer treatment using radiolabeled NOTA-hTf in advance, it will become possible to provide the best cancer treatment for each patient.

Funding

This work was supported by Grant-in-Aids for Scientific Research from the Japan Society for the Promotion of Science [19H04264 (HY)].

Author contributions

Conception and design of study: H.Y., Y.K., Acquisition of data: Y.S., H.Y., K.H., Drafting the manuscript: Y.S., H.Y., and Y.K.

Declaration of competing interest

The authors declare that they have no known competing financial interests or personal relationships that could have appeared to influence the work reported in this paper.

Acknowledgements

We thank ATOX Co., Ltd. for providing the ^{68}Ge/^{68}Ga-generator used in the study. We are also deeply grateful to the staff members of the Central Institute of Isotope Science, Hokkaido University for their skillful technical assistance.

Appendix A. Supplementary data

Supplementary data related to this article can be found at https://doi.org/10.1016/j.bbrep.2021.100957.

References

[1] C. Swanton, Intratumor heterogeneity: evolution through space and time, Canc. Res. 72 (2012) 4875–4882, https://doi.org/10.1158/0008-5472.can-12-2217.
[2] C. Holohan, S. Van Schaeybroeck, D.B. Longley, P.G. Johnston, Cancer drug resistance: an evolving paradigm, Nat. Rev. Canc. 13 (2013) 714–726, https://doi.org/10.1038/nrc3599.
[3] S.J. Dixon, K.M. Lemberg, M.R. Lamprecht, et al., Ferroptosis: an iron-dependent form of nonapoptotic cell death, Cell 149 (2012) 1060–1072, https://doi.org/10.1016/j.cell.2012.03.042.
[4] L.M. Bystrom, S. Rivella, Cancer cells with irons in the fire, Free Radic. Biol. Med. 79 (2015) 337–342, https://doi.org/10.1016/j.freeradbiomed.2014.04.035.
[5] H.L. Elford, M. Freese, E. Passamani, H.P. Morris, Ribonucleotide reductase and cell proliferation. I. Variations of ribonucleotide reductase activity with tumor growth rate in a series of rat hepatomas, J. Biol. Chem. 245 (1970) 5228–5233. https://www.ncbi.nlm.nih.gov/pubmed/4319235.
[6] M. Conrad, J.P. Angeli, P. Vandenabeele, B.R. Stockwell, Regulated necrosis: disease relevance and therapeutic opportunities, Nat. Rev. Drug Discov. 15 (2016) 348–366, https://doi.org/10.1038/nrd.2015.6.
[7] M. Luo, L. Wu, K. Zhang, et al., miR-137 regulates ferroptosis by targeting glutamine transporter SLC1A5 in melanoma, Cell Death Differ. 25 (2018) 1457–1472, https://doi.org/10.1038/s41418-017-0053-8.
[8] W.S. Yang, R. SriRamaratnam, M.E. Welsch, et al., Regulation of ferroptotic cancer cell death by GPX4, Cell 156 (2014) 317–331, https://doi.org/10.1016/j.cell.2013.12.010.
[9] B. Lu, X.B. Chen, M.D. Ying, et al., The role of ferroptosis in cancer development and treatment response, Front. Pharmacol. 8 (2017) 992, https://doi.org/10.3389/fphar.2017.00992.
[10] W.S. Yang, B.R. Stockwell, Synthetic lethal screening identifies compounds activating iron-dependent, nonapoptotic cell death in oncogenic-RAS-harboring cancer cells, Chem. Biol. 15 (2008) 234–245, https://doi.org/10.1016/j.chembiol.2008.02.010.
[11] M. Gao, P. Monian, N. Quadri, et al., Glutaminolysis and transferrin regulate ferroptosis, Mol. Cell. 59 (2015) 298–308, https://doi.org/10.1016/j.molcel.2015.06.011.
[12] J.P. Holland, M.J. Evans, S.L. Rice, et al., Annotating MYC status with 89Zr-transferrin imaging, Nat. Med. 18 (2012) 1586–1591, https://doi.org/10.1038/nm.2935.
[13] S. Bhattacharyya, S. Bhattacharyya, L. Wei, J. Shi, Synthesis of USP-grade 89Zr-panitumumab for medical use, Protoc. Exch. (2013) 1–16, https://doi.org/10.1038/protex.2013.077.
[14] L. Perk, G. Visser, M. Budde, et al., Facile radiolabeling of monoclonal antibodies and other proteins with zirconium-89 or gallium-68 for PET imaging using p-isothiocyanatobenzyl-desferrioxamine, Nat. Protoc. (2008), https://doi.org/10.1038/nprot.2008.22.
[15] I. Velikyan, 68Ga-based radiopharmaceuticals: production and application relationship, Molecules 20 (2015) 12913–12943, https://doi.org/10.3390/molecules200712913.

[16] C. Truillet, J.T. Cunningham, M.F.L. Parker, et al., Noninvasive measurement of mTORC1 signaling with ^{89}Zr-transferrin, Clin. Canc. Res. 23 (2017) 3045–3052, https://doi.org/10.1158/1078-0432.ccr-16-2448.
[17] J.L. Roh, E.H. Kim, H.J. Jang, et al., Induction of ferroptotic cell death for overcoming cisplatin resistance of head and neck cancer, Canc. Lett. 381 (2016) 96–103, https://doi.org/10.1016/j.canlet.2016.07.035.
[18] Y. Yu, Y. Xie, L. Cao, et al., The ferroptosis inducer erastin enhances sensitivity of acute myeloid leukemia cells to chemotherapeutic agents, Mol. Cell Oncol. 2 (2015), e1054549, https://doi.org/10.1080/23723556.2015.1054549.
[19] L. Chen, X. Li, L. Liu, et al., Erastin sensitizes glioblastoma cells to temozolomide by restraining xCT and cystathionine-γ-lyase function, Oncol. Rep. 33 (2015) 1465–1474, https://doi.org/10.3892/or.2015.3712.
[20] M. Gao, P. Monian, Q. Pan, et al., Ferroptosis is an autophagic cell death process, Cell Res. 26 (2016) 1021–1032, https://doi.org/10.1038/cr.2016.95.
[21] S. Young, A. Bomford, Transferrin and cellular iron exchange, Clin. Sci. 67 (1984) 273–278, https://doi.org/10.1042/cs0670273.
[22] S.L. Byrne, P.D. Buckett, J. Kim, et al., Ferristatin II promotes degradation of transferrin receptor-1 in vitro and in vivo, PLoS One 8 (2013), https://doi.org/10.1371/journal.pone.0070199.
[23] W.S. Yang, K.J. Kim, M.M. Gaschler, et al., Peroxidation of polyunsaturated fatty acids by lipoxygenases drives ferroptosis, Proc. Natl. Acad. Sci. Unit. States Am. 113 (2016) E4966–E4975, https://doi.org/10.1073/pnas.1603244113.
[24] F. Ye, W. Chai, M. Xie, et al., HMGB1 regulates erastin-induced ferroptosis via RAS-JNK/p38 signaling in HL-60/NRAS, Am. J. Cancer Res. 9 (2019) 730–739. https://www.ncbi.nlm.nih.gov/pubmed/31105999.